Bertolesi, E.; Buitrago, M.; Giordano, E.; Calderón García, PA.; Moragues, JJ.; Clementi, F.; Adam, JM. (2020). Effectiveness of Textile Reinforced Mortar (TRM) Materials in preventing Seismic-Induced Damage in a U-Shaped Masonry Structure Submitted to Pseudo-Dynamic Excitations. Construction and Building Materials. 248:1-17. https://doi.org/10.1016/j.conbuildmat.2020.118532

Effectiveness of Textile Reinforced Mortar (TRM) Materials in preventing Seismic-Induced Damage in a U-Shaped Masonry Structure Submitted to Pseudo-Dynamic Excitations

Elisa Bertolesi*[a], Manuel Buitrago[a], Ersilia Giordano[b], Pedro A. Calderón[a], Juan J. Moragues[a], Francesco Clementi[b], José M. Adam[a]

[a]ICITECH, Universitat Politècnica de Valencia, Camino de Vera s/n, 46022, Valencia, Spain

[b] Department of ICEA, Università Politecnica delle Marche, Ancona, Italy

*Corresponding author: elber4@upv.es

Abstract

This paper presents the experimental results obtained from tests on a 2/3 scale U-shaped masonry building constructed in one of the *ICITECH* laboratories at the *Universitat Politècnica de València* (Spain). The prototype measured 3.31x4.19 m^2 by 2.15 m high and had a wall thickness of 230 mm. The masonry was composed of 230x110x50 mm^3 solid clay bricks with approximately 10 mm-thick mortar joints arranged in English bond. The tests were aimed at evaluating the effectiveness of cement-based reinforcing materials (Textile Reinforced Mortar) applied to weak masonry substrates severely damaged by horizontal loads such as those induced by a seismic event. The tests were carried out in three phases: (i) testing of the as-built structure, (ii) application of one external layer of TRM to restore the masonry's original load-bearing capacity and then (iii) testing the TRM-strengthened structure. Dynamic behaviour was monitored by both traditional and fibre optic sensors (FO), including 28 Linear Variable Displacement Transducers (LVDTs) and 3 long-gauge optical sensors. Strengthening effectiveness was evaluated by several parameters: hysteretic curves, strength degradation, computed cumulative energy dissipation and cracking mechanisms. TRM reinforcement was shown to significantly extend the load-bearing and displacement capacity of the masonry prototype, reducing seismic-induced damage applied by pseudo-dynamic excitation, although it had a limited effect on cumulative energy dissipation.

Keywords: Textile Reinforced Mortar (TRM), In-Scale Masonry Structure, Experimental Pseudo Dynamic Tests, Seismic Performance.

1. Introduction

Old masonry buildings are often constructed of locally available clay/stone blocks and mortar joints with a wide range of mechanical properties, which makes it difficult to predict their ultimate bearing capacity. These structures were usually designed to sustain only compressive loads and were built by intuitive rules of thumb without any regard to the current seismic guidelines, and during earthquakes they tended to be quite vulnerable to out-of-plane mechanisms without reaching their full load bearing capacity [1][2][3]. The activation of this type of failure is often imputed to different parameters, namely: (i) weak connections between lateral and transversal walls, (ii) no box behaviour, (iii) geometrical asymmetries and thus high torsional effects, (iv) poor mechanical behaviour of the masonry assemblage, (v) high masses, and thus powerful inertial effects, and finally (vi) limited ductility [1][2][3].

Different reinforcing materials have recently been proposed to overcome these issues, the two most important organic and inorganic-based types are: Fibre Reinforced Polymer composites (also known as FRP) [4] which pertain to the first group, since they include an epoxy resin matrix, and Textile Reinforced Mortar (TRM or FRCM) materials [5]. In both cases, the strengthening is composed of a strong heterogeneous combination of two materials: a matrix (resin or cement mortar) and a high-performance strips or a network of continuous-fibre textile (i.e. carbon, glass or aramid).

FRP materials were developed especially to exploit carbon fibre's tensile properties by ensuring a perfect epoxy bond between net and supports. Thanks to their ability to impregnate porous media such as concrete and masonry, organic matrices attracted the attention of researchers and practitioners, so that FRP composites were first adopted to strengthen concrete structures as well as to improve their flexural or shear capacities, following the current structural guidelines. Their efficiency relies on the capacity of the matrix to transfer tangential stresses from the support to the textile fibres, which are designed to bear tensile loads only. The quality of the bond clearly plays a crucial role in ensuring that the strengthening works properly, increasing stiffness and structural strength, as well as their displacement capacity, and thus avoiding premature abrupt failures [4][6][7]. Various research groups have studied the effects of applying FRP composites to concrete structures [4] as well as to isolated structural elements [6][7] subjected to different loading conditions. One of the most critical failure modes encountered in FRP-repaired structures is due to the so called "delamination phenomenon". As described in [8], this failure mechanism frequently involves the propagation of a debonding front, accompanied by the removal of a variable layer of the support, depending on the quality of the substrate.

Due to their multiple advantages, such as high strength, high elastic modulus, low mass, high ductility, ease of application and durability, FRP materials seemed to offer a promising solution

for the repair of masonry structures. They were first used to strengthen old masonry buildings in seismic-prone areas suffering from structural deficiencies when subjected to horizontal loads. Several research groups have analysed the efficacy of FRP composites applied to brittle supports, including [9]-[13], which are some of the leading studies in the last ten years.

Although they showed high performance, FRPs also revealed some serious drawbacks, especially when applied to historical masonry structures, as the epoxy resin was quite aggressive with masonry assemblages. Indeed, deep impregnation of the support can modify their chemical structure and make the epoxy almost impossible to remove, besides changing the hydrothermal regulation capacity of the masonry itself. They thus became rapidly unusable as a strengthening solution for the architectural heritage and were not recommended by the responsible bodies, such as the Italian Cultural Heritage Ministry [14].

As a result of the recent renewal of the architectural heritage conservation principles, such as minimal intervention, reversibility, compatibility and durability, a different type of composite was developed. The idea was to maintain the high performance of the lightweight textile fibre net, while replacing the polymeric matrix with a more compatible mortar binder in the form of Fibre Reinforced Cementitious Matrix (FRCM) materials and Textile Reinforced Mortar (TRM) composites [5]. Unlike FRPs, TRMs allow the masonry to breathe while ensuring good adhesion, while the peculiar failure mode of cementitious-based materials ensures more ductile masonry behaviour, as pointed out in [15][16]. Many studies have evaluated the capacity of TRM to prevent both in and out-of-plane collapses [15]-[19]. However, little work has been done to evaluate the overall effect of cementitious-based materials applied to scaled-down or full-scale masonry buildings, since these tests are costly in terms of money and time [20]-[23].

The present paper fits into the latter category and describes a double experimental campaign designed to evaluate the strengthening effectiveness of a glass-textile TRM material applied to a one-storey U-shaped masonry building with window and door openings of different sizes. The building itself was made of clay bricks with 10 mm-thick mortar joints arranged in English bond. The masonry prototype was subjected to a pseudo-dynamic cyclic test on the as-built and TRM-repaired structures to analyse the overall effect of cementitious-based materials in the presence of dynamic loads.

The paper is organised as follows: Section 2 describes the construction of the masonry building and the repairs carried out after the first test, as well as the preliminary lab tests to characterize the mechanical properties of the masonry constituents and TRM strengthening materials. Section 3 describes the loading protocol and the monitoring system and sensors. Section 4 analyses the experimental results of the tests on the control and TRM-reinforced buildings and the outcomes of the buildings' structural response in terms of: strength degradation, pinching

effect, hysteretic and envelope curves and cracking mechanisms, while Section 5 summarizes the laboratory outcomes and possible future research lines.

2. Experimental tests

The experimental campaign was carried out at the *Universitat Politècnica de València* (Valencia, Spain) on a one-storey masonry building subjected to horizontal pseudo-dynamic excitation. This section is organized into three parts: (i) a description of the as-built prototype, (ii) a description of the Textile Reinforced Mortar (TRM) strengthening technique adopted to repair the damaged building, and (iii) an analysis of the mechanical characterization of the constituent materials.

2.1 U-Shaped Unreinforced Masonry Building

A 2/3 scale one-floor masonry structure was built of 230x110x50mm^3 solid clay bricks with 10 mm thick mortar joints, arranged in a typical English bond pattern, as depicted in Figure 1.

-a

-b

Figure 1: English bond masonry assemblage: front view (-a) and corner detail (-b).

The building was U-shaped and contained window and door openings. The walls were 2.15 m high with a constant thickness of 230 mm. The building comprised three panels: a solid transversal wall and two side panels labelled *Wall A, Wall B* and *Wall C*, respectively (see Table 1 and Figure 2).

	H [m]	L [m]	T [m]	H [m]	L [m]	Aspect ratio[H/L]	Slenderness ratio[H/t]	Opening ratio [h*l/H*L]
Solid wall (Wall A)	2.15	4.19	0.23	/	/	0.51	9.35	0.00
Lateral wall with door (Wall B)	2.15	3.11	0.23	1.37	0.97	0.69	9.35	0.20
Lateral wall with window (Wall C)	2.15	3.11	0.23	0.78	0.97	0.51	9.35	0.11

Table 1: Geometrical parameters of the tested masonry building.

It is important to underline that, structure-wise, old masonry buildings are often prone to out-of-plane failures when subjected to seismic actions. This is commonly triggered by the lack of box behaviour due to the absence of strong connections at the corners and the considerable deformability of the horizontal diaphragms. In order to study the vulnerability of the corner connection of traditional English bond masonry structures subjected to horizontal loads, no rigid floors were adopted, as the authors preferred a lighter solution composed of 720 mm spacing concrete joists and hollow concrete blocks simply supported on the lateral walls only. The roof elements are depicted in Figure 2 together with their main geometrical dimensions. 1450x130x230 mm^3 wooden lintels were used to bear the vertical loads of the masonry above each opening (see Figure 2 – Detail A). The masonry construction was firmly anchored to the reaction floor by a system of thin steel plates. The steel bases (see Figure 2 – Detail C) were designed to avoid undesired sliding of the structure when subjected to horizontal loads.

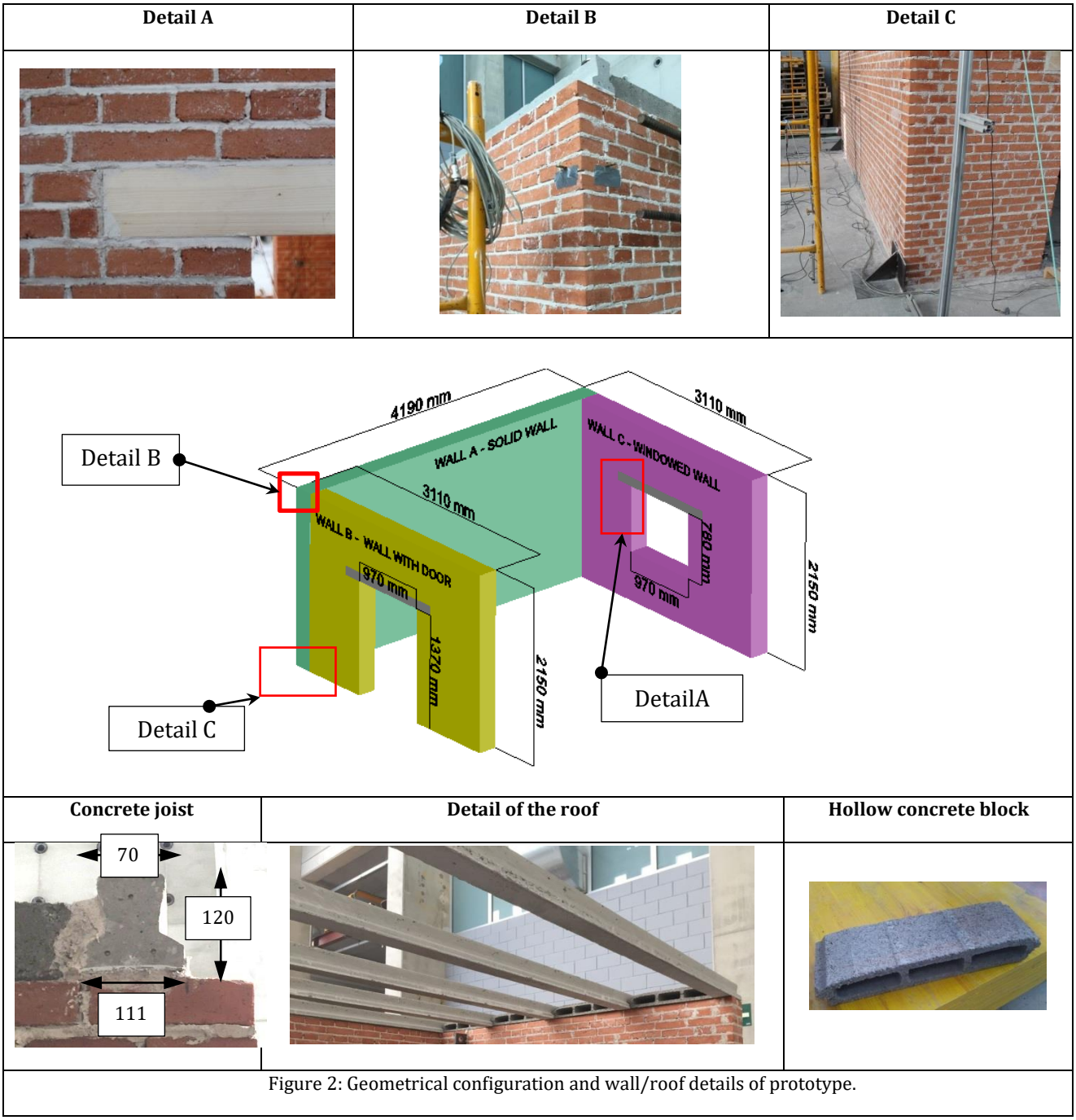

Figure 2: Geometrical configuration and wall/roof details of prototype.

2. 2 TRM Strengthening Phases

The tests were divided into two parts: (i) the application of a series of cyclic pseudo-dynamic excitations to the unreinforced prototype, and then (ii) the repetition of a partially extended loading protocol on the TRM-reinforced masonry structure. Before applying the TRM reinforcement, the masonry support was restored to its original load-bearing capacity. The retrofitting involved the following phases: (i) drilling 20-40 mm holes through approximately 2/3 of the wall thickness, (ii) positioning the plastic injectors (Figure 3-a), (iii) filling external

cracks to avoid slurry leaks (Figure 3-b and -c), (iv) injection of super-fluid slurry and (v) removal of the plastic injectors (Figure 3-d).

-a

-b

-c

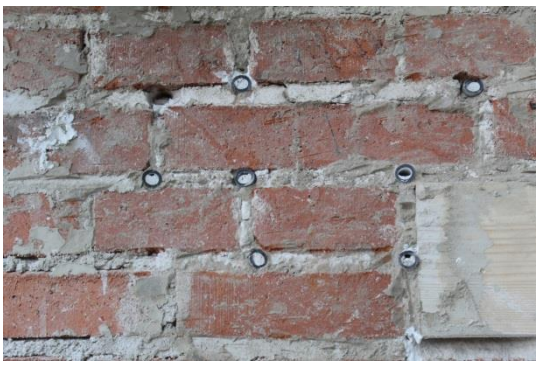

-d

Figure 3: TRM strengthening phases: positioning of the injectors (-a), filling with mortar (-b), consolidation of the windowed wall (-c) and final appearance (-d).

During the second step, the whole external surface of the building was covered with an approximately 10 mm thick layer of glass TRM (Textile Reinforced Mortar) composite with a 25 mm spacing balanced glass textile grid [24]. The TRM was applied in four steps comprising: (i) washing the masonry support, (ii) application of 5mm thick layer of cementitious mortar to the masonry support, (iii) placing strips of glass textile and (iv) applying a finishing 5 mm thick cementitious mortar layer.

2.3 Mechanical Characterisation of Constituent Materials

This section contains the experimental results of the tests on the constituent materials used for the construction and repair of the masonry prototype. These materials (lime mortar and solid bricks) and the TRM cementitious binder were analysed by means of a series of three-point bending and compressive tests. Four randomly selected bricks were tested to characterize their flexural strength (three-point bending tests), after which the four halves obtained were subjected to a direct compression test to evaluate their peak compressive strength and Elastic

Modulus. For this, two Linear Variable Displacement Transducers (LVDTs) were placed between two stiff steel plates to uniformly apply a vertical compressive load on the specimens. The Elastic Modulus was calculated as the slope of the third compression loading cycle according to EN 14580 [25].

Six 40 × 40 × 160 mm^3 prismatic specimens were poured into a custom-made iron mould. Four were given a three-point bending test and a compression test after 28 days of curing, and the other two were characterized after 108 days (ages coincide with the pseudo-dynamic tests on the building) according to EN 13412 [26], while the compression tests were conducted according to EN1015-11 [27] and the Elastic Modulus following EN 14580 [25]. The compression tests were performed on 40 × 40 × 40 mm^3 cubic specimens.

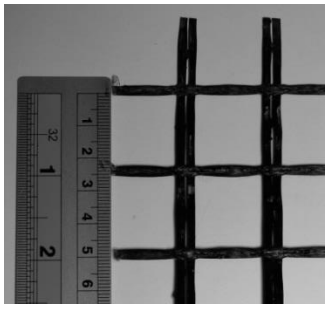

Mesh size	25 x 25	[mm]
Weight	225	[g/mm^2]
Density of fibre	2.5	[g/cm^3]
Tensile strength	45	[kN/m]
Modulus of elasticity	72	[GPa]
Resistant Area	35.27	[mm^2/m]

Table 2: Mechanical properties of textile glass as furnished by the manufacturer [24].

The TRM used to strengthen the masonry prototype was composed of a balanced glass grid and two 5 mm thick layers of cementitious mortar. The glass textile consisted of a 25 mm spacing alkali-resistant glass grid with an equivalent resistant area of 35.27 mm^2/m. Its mechanical properties can be seen in Table 2 [24]. Similarly to the lime mortar, the TRM cement binder was poured into 40 × 40 × 160 mm^3 and 40 × 40 × 40 mm^3iron moulds for the three-point bending and compression tests, respectively, as per EN 1015-11 [27] and EN 13412 [26]. The elastic modulus was calculated following EN 14580 [25].

The experimental outcomes obtained at the end of the series of three-point bending tests and compression tests are listed in Table 3.

CLAY BRICK					
	Three-point bending test		**Compression test**		
		$\sigma_{f,max}$ [MPa]		E [MPa]	$\sigma_{c,max}$ [MPa]
	Test 1	4.33	Test 1	800.13	11.38
	Test 2	4.92	Test 2	1332.68	14.89
	Test 3	3.26	Test 3	999.45	16.04
	Test 4	5.15	Test 4	989.30	13.64
MEAN VALUE		**4.42**		**1030.39**	**14.00**
LIME MORTAR					
At 28 days	Test 1	1.11	Test 1	789.98	4.11
	Test 2	1.62	Test 2	810.83	3.90
	Test 3	1.76	Test 3	728.35	4.66
	Test 4	1.42	Test 4	578.17	4.33
MEAN VALUE		**1.48**		**726.83**	**4.25**
At 108 days	Test 1	1.05	Test 1	922.02	4.90
	Test 2	1.23	Test 2	1202.06	7.07
MEAN VALUE		**1.14**		**1062.04**	**6.0**
TRM CEMENTITIOUS MORTAR					
At 63 days	Test 1	4.71	Test 1	3949.47	17.10
	Test 2	5.52	Test 2	3032.25	17.45
	Test 3	5.79	Test 3	3592.14	17.50
	Test 4	4.65	Test 4	1573.70	17.25
	Test 5	5.07	Test 5	4513.32	16.60
	Test 6	6.15	Test 6	2416.45	17.04
MEAN VALUE		**5.315**		**3179.55**	**17.16**

Table 3: Mechanical properties of clay bricks, lime mortar and TRM cementitious mortar.

3. Test Protocol

The masonry structure was subjected to a series of cycles by means of a servo hydraulic jack positioned on the free edge of the U-shaped building, which generated the cycles by imposing positive (Pull) and negative (Push) displacements on the structure. To analyse the effect of the dynamic excitation on the masonry, the horizontal loads were applied by a stiff steel beam connecting the two side walls and the horizontal jack. The torsional effect of the building due to the different stiffness of the lateral walls was also considered by placing a cylindrical hinge between the steel beam and the hydraulic jack (see Figure 4). The loading during the tests was also recorded by means of a load cell between the hydraulic jack and the hinge.

-a -b

Figure 4: Details of the loading system: hydraulic jack with central hinge (-a) and anchorage to the masonry prototype (-b).

A total of 6 (225 cycles) and 7 (149 cycles) series of pseudo-dynamic excitations, each lasting 10 seconds, were applied to the unreinforced (URM) and TRM-strengthened structures. Figure 5 summarises both tests in all the series of dynamic excitations, horizontal displacements imposed by the hydraulic jack on the side panels, and the associated excitation frequencies.

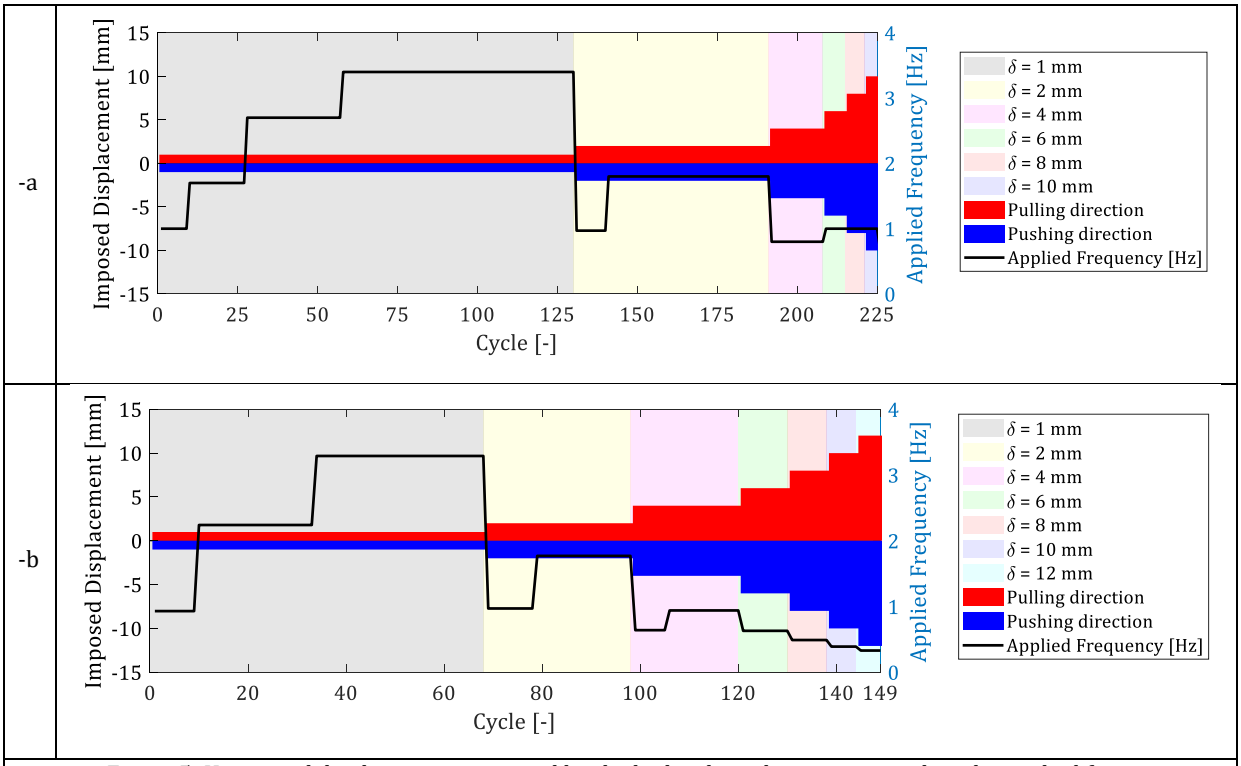

Figure 5: Horizontal displacements imposed by the hydraulic jack superimposed on the applied frequency, considering: the as-built building (-a) and the TRM reinforced building (-b).

The imposed displacements ranged between ±1 mm to ±12 mm, while the applied frequencies varied between 0.4 Hz up to 4 Hz. Two series of tests were conducted considering two different configurations: (i) the unreinforced masonry structure (URM) and (ii) the TRM - reinforced structure. The masonry prototype was monitored by a total of 28 LVDTs and 3 FOS. The LVDTs were placed on the internal and external surfaces of the prototype as shown in Figure 6. The most likely cracking patterns were characterized by the widening of stepped cracks close to the corners of the building and those of the door and window openings due to the activation of a possible out-of-plane mechanism in the solid wall. Most of the LVDTs were thus placed on the corner diagonals (LVDTs 1-2-3-4-5-6-12-13-14-15), while the four vertical LVDTs (6-7-16-17) were fixed to the lintels to capture the possible detachment of the wooden beam from the masonry panels. Horizontal LVDTs 9-10-11-18-19-20 were placed between the solid and side walls to monitor a possible overturning mechanism in the transversal wall. Seven LVDTs (XE1-XE2-ZE1-ZE2-ZE3-ZE4 and ZE5) monitored the overall behaviour of the building and its torsional effect during the pseudo-dynamic excitations.

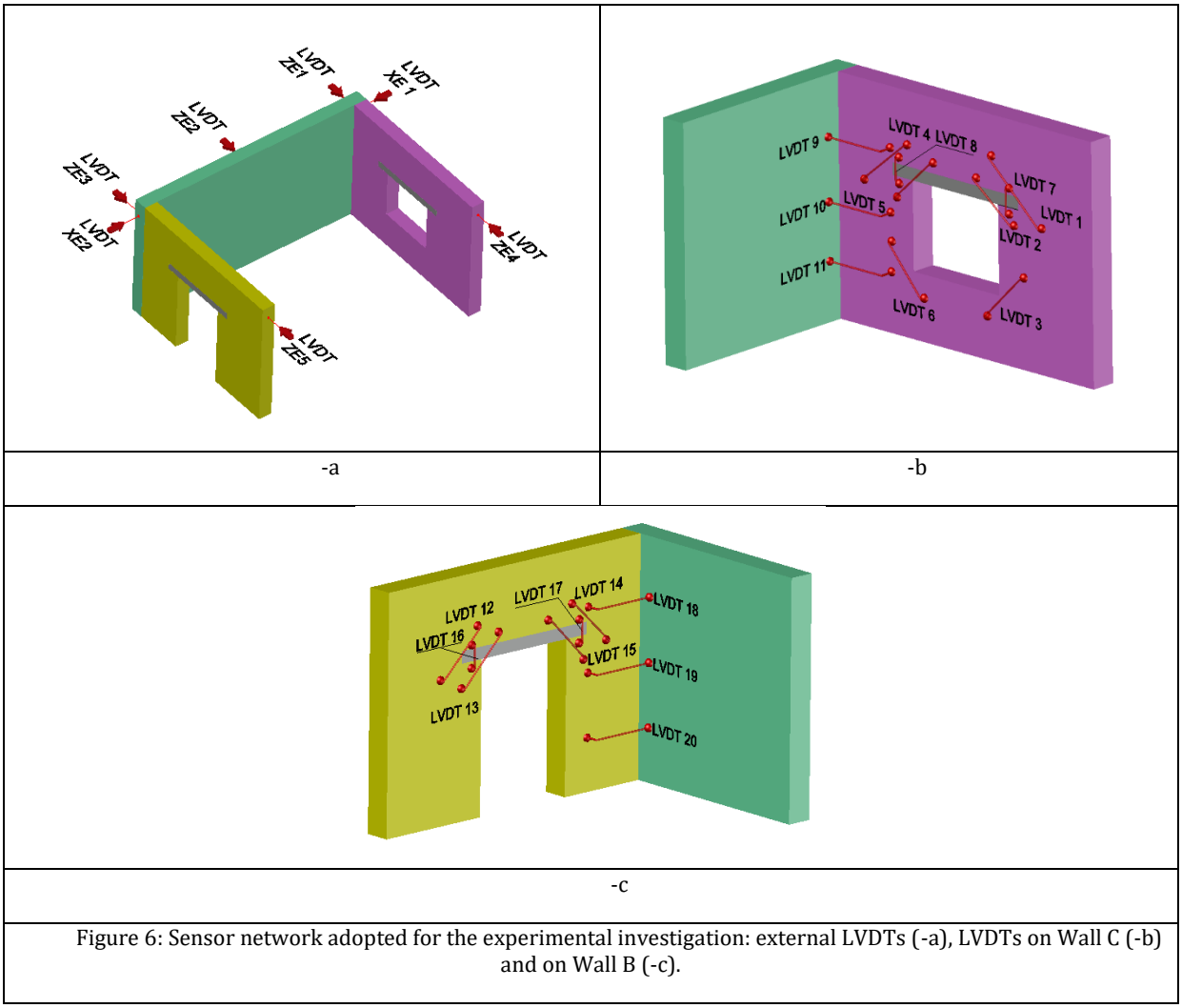

-a

-b

-c

Figure 6: Sensor network adopted for the experimental investigation: external LVDTs (-a), LVDTs on Wall C (-b) and on Wall B (-c).

4. Experimental Results

This section is organized into five parts for five specific aspects of the pseudo dynamic loading: strength degradation, pinching effect, cumulative energy dissipation, and cracking mechanism. The results are superimposed on the set of displacements applied during the tests for the as-built and TRM reinforced cases.

4.1 As-built Prototype

4.1.1 Strength Degradation

The strength degradation values shown in Figure 7 were computed from the maximum reaction forces read by the load cell in each cycle during the hydraulic jack's pulling and pushing actions. The behaviour of the masonry building can be seen to be quite symmetric (±20 kN) at low displacement values (up to 2 mm). As expected, the reaction forces increased with the imposed displacement, meaning that up to 4 mm negligible damage mechanisms took place.

After 4 mm, the structural behaviour of the as-built prototype clearly experienced strength degradation when subjected to pushing loads. Two different mechanisms can be seen from 4 mm till the end of the test: (i) reaction forces increased as the imposed displacement increased, but not in proportion, and (ii) different strength degradation trends were observed at each level of the imposed displacement. It should be noted that each displacement set was characterized by a steeper strength degradation slope as the cracking mechanism progressively worsened the building's structural response. This behaviour was also seen during pulling loads. Indeed, after 4 mm, the pulling forces did not increase with displacement, which could be explained by the cracking mechanism which spread to the loading areas and threatened the transmission of the pulling force to the building.

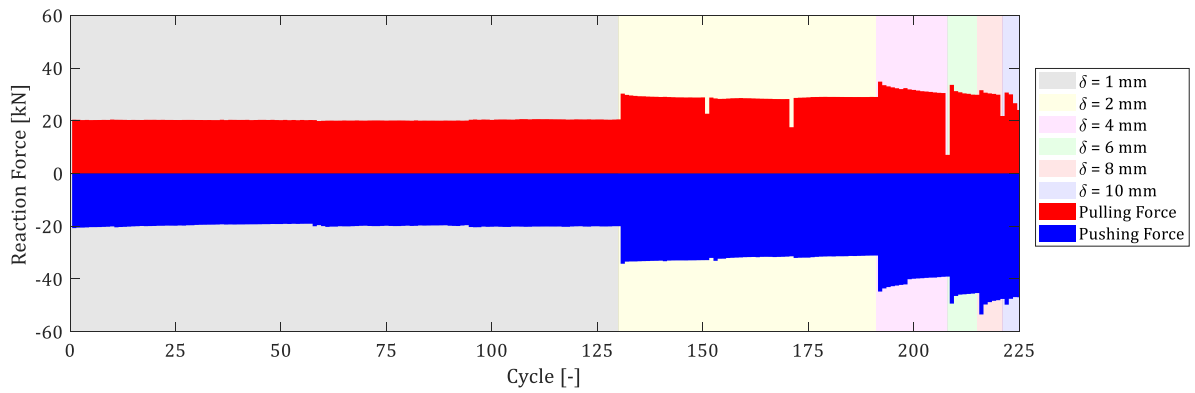

Figure 7: Strength degradation values obtained in tests on the as-built building.

4.1.2 Pinching Effect

Pinching is a well-recognized effect in structures subjected to cyclic loads and the results obtained clearly show this behaviour (see Figure 8), which gives the absolute values of the difference between the displacements at peak load and the residual values at the end of each unloading phase, as recorded by LVDTs ZE1, ZE3, ZE4 and ZE5. The values were calculated separately for pulling and pushing loads. As can be noted, pinching was detected both under pulling and pushing actions and was more pronouncedly in ZE4 and ZE5. The different behaviour tracked by ZE1 and ZE3 under pulling actions is explained by the cracking mechanism, which propagated to the loading areas, thus threatening the transmission of the pulling loads. Under pushing actions, the four LVDTs recorded similar values. Figure 8 clearly shows pinching in the second set of displacements (2 mm). The comparison between the results in Figure 8-a and –c under pushing loads shows similar displacement trends, with a final maximum value around 4 mm. Figure 8-b and –d also show quite high displacement values of almost 7 mm. This different behaviour could be explained by the different stiffness of the door and window panels and thus by the activated torsional effect.

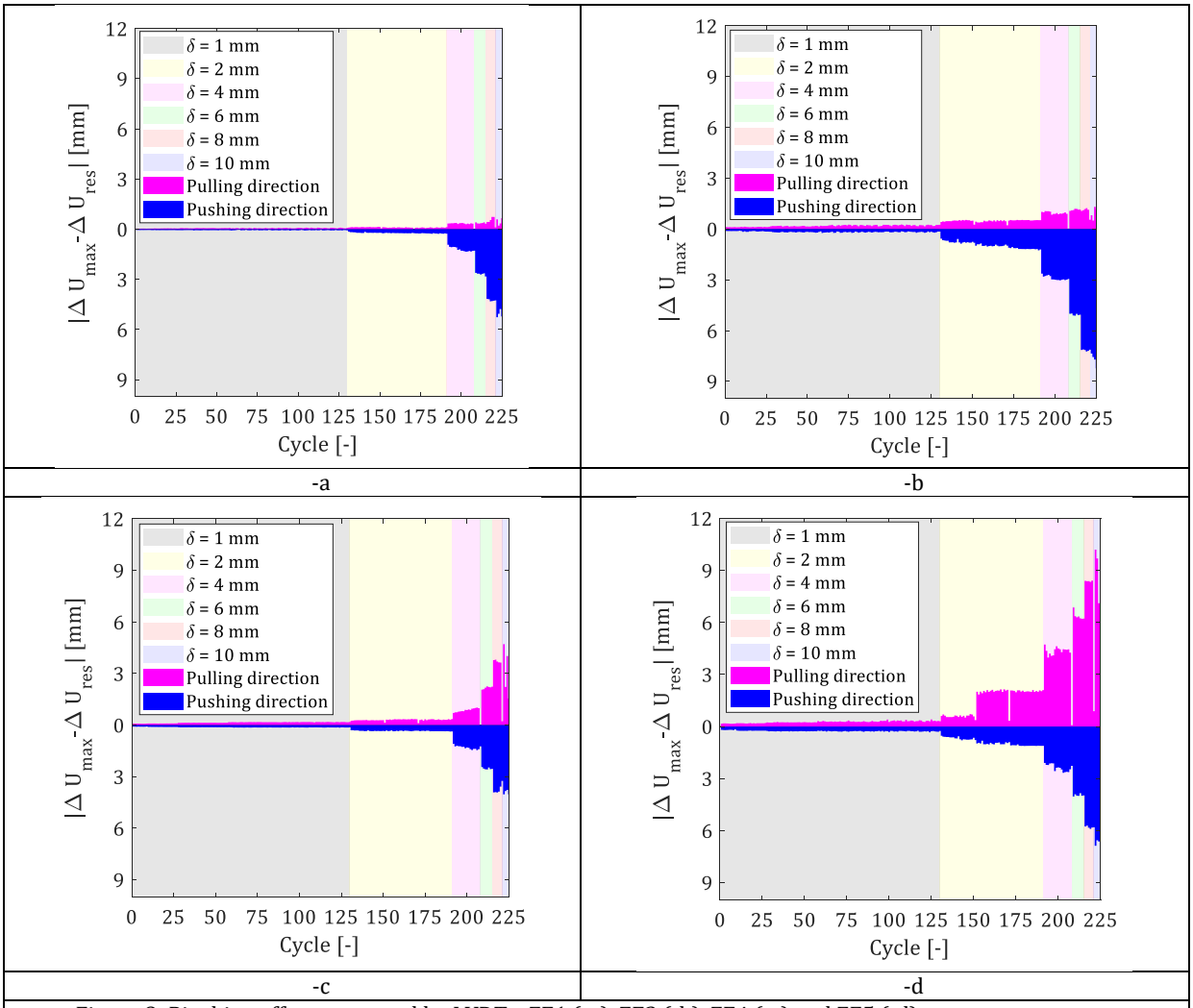

Figure 8: Pinching effect computed by LVDTs: ZE1 (-a), ZE3 (-b), ZE4 (-c) and ZE5 (-d).

Pinching effects were also visible in the hysteretic curves detected by the four LVDTs. Figure 9 shows the force-displacement curves obtained in the last cycle of each set of imposed displacements. Pinching is clearly visible from the second set of displacements (2 mm). ZE4 and ZE5 show a clear almost symmetric behaviour under pulling and pushing actions, as reflected by the analyses in Figure 8-c and –d.

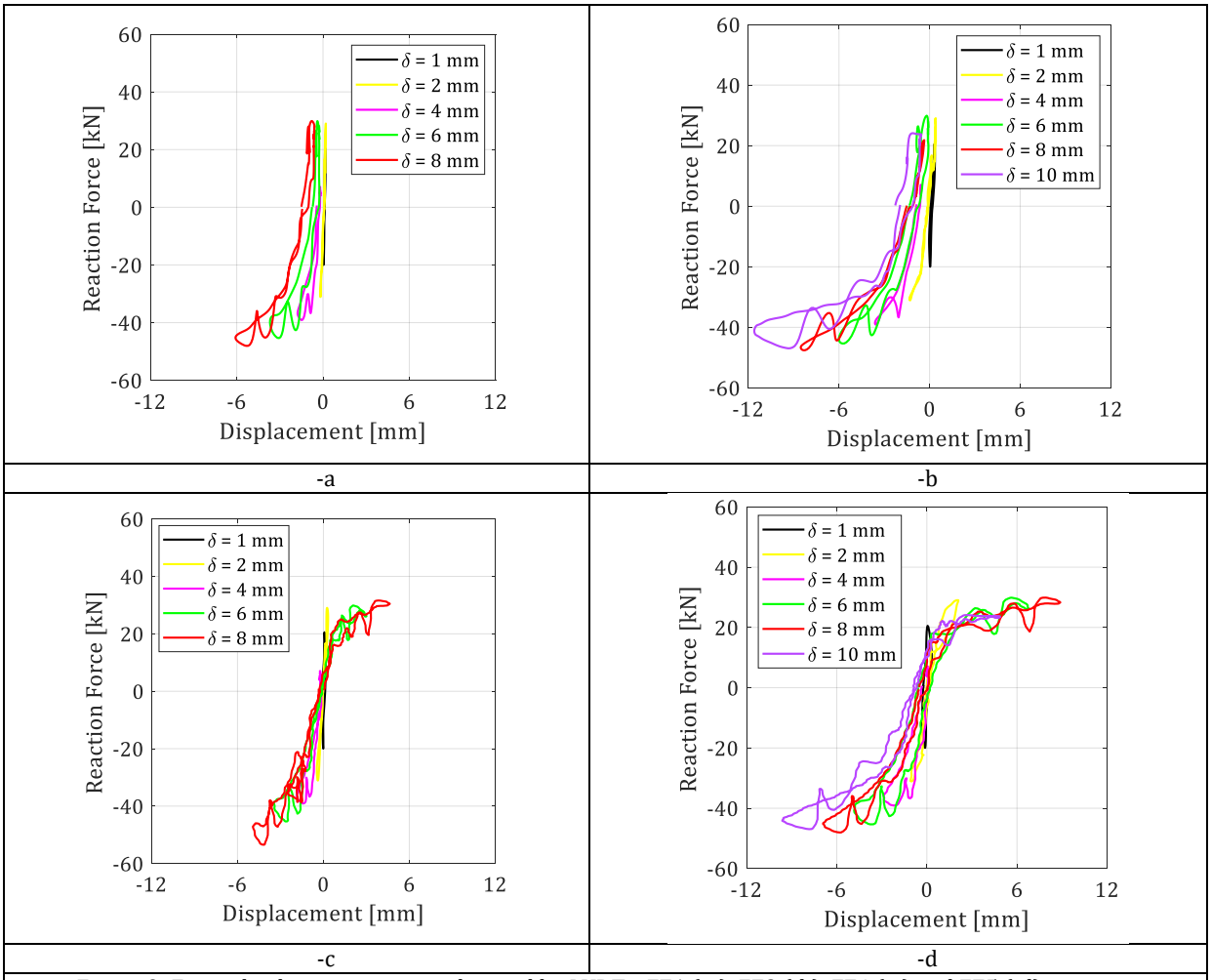

Figure 9: Force-displacement curves obtained by LVDTs: ZE1 (-a), ZE3 (-b), ZE4 (-c) and ZE5 (-d).

4.1.3 Cumulative Energy Dissipation

Cumulative Energy Dissipation (CED) was computed as the area enclosed by each hysteretic curve numerically integrated by a trapezoidal rule. The results obtained for displacements by ZE1, ZE3, ZE4 and ZE5 are given in Figure 10. The cycles in which damage threatened the load transmission were excluded from the calculation of cumulative energy dissipation. As can be noted in Figure 10, ZE5 (Wall B) dissipated a substantially higher amount of energy than the other LVDTs, in particular more than ZE4. This trend is also reflected by ZE3 (Figure 10-b), which shows a relatively higher CED than ZE1 (Figure 10-a) due to the cracking mechanisms in the two side walls. Although Wall C presented a more severe final cracking pattern with stepped cracks in almost all the corners of the window, Wall B entered the stage of elastic–plastic deformation earlier (around the 125th cycle). In fact, Wall C only started cracking around the 200th cycle (4 mm) and from then on the cumulative energy dissipation trends monitored by all the LVDTs increased with a clearly higher rate.

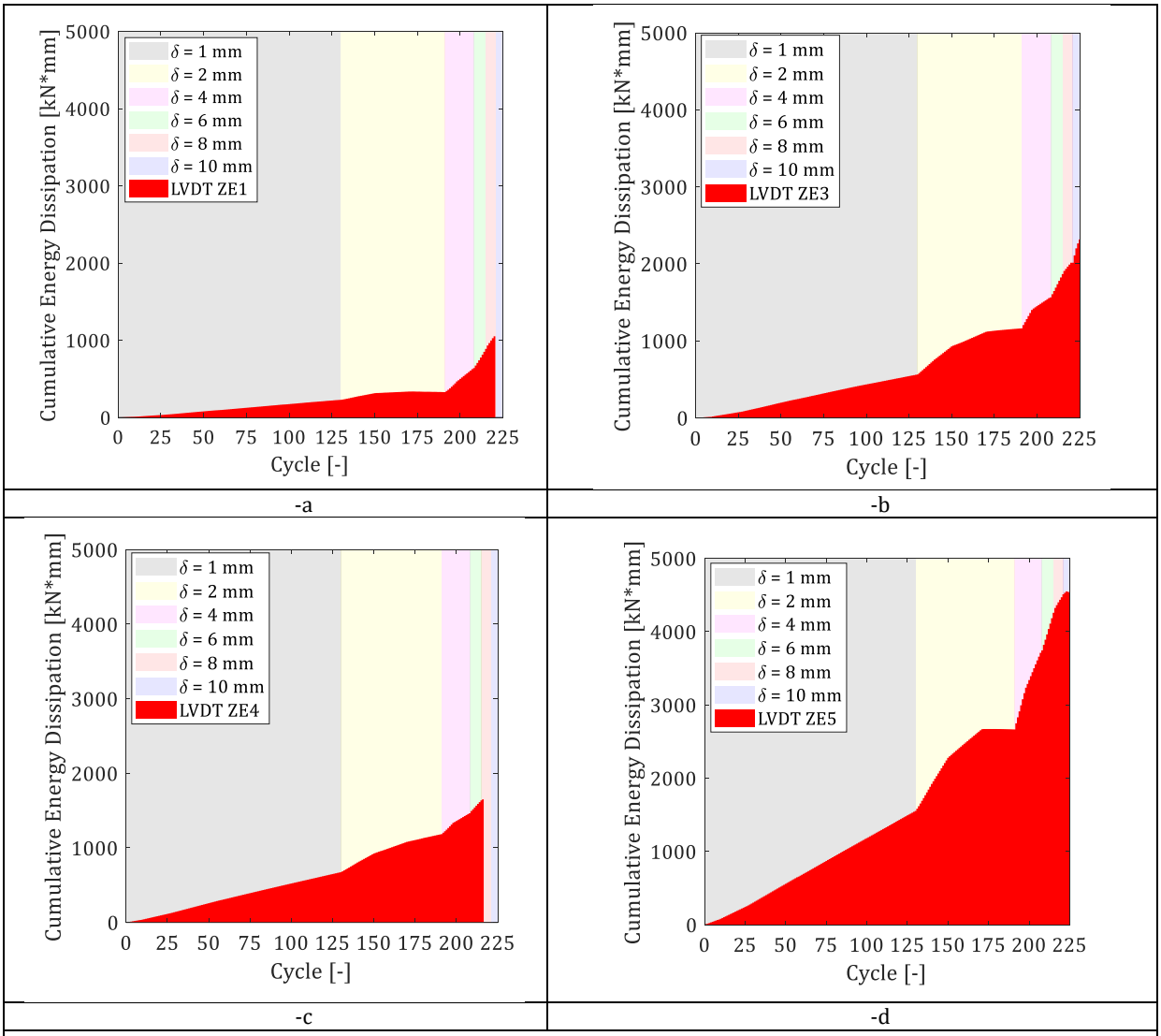

Figure 10: Cumulative energy dissipation evaluated using LVDTs: ZE1 (-a), ZE3 (-b), ZE4 (-c) and ZE5 (-d).

4.1.4 Envelopes

The envelope curves connecting peak loads and the associated displacements of the hysteretic curves from ZE1, ZE3, ZE4 and ZE5 can be seen in Figure 11. Only compressive displacements were considered since the pulling displacements recorded by ZE1 and ZE3 were affected by the damaged masonry , while both pulling and pushing envelope curves are shown in Figure 11-c and –d. Reasonably symmetric behaviour was obtained from these envelopes, with slightly higher reaction forces under pushing loads (also see Figure 7). Different strength degradation trends can be distinguished in both types, characterized by: (i) a slight reduction of the peak forces as displacement increases under pushing actions and (ii) a constant trend with negligible strength degradation under pulling loads.

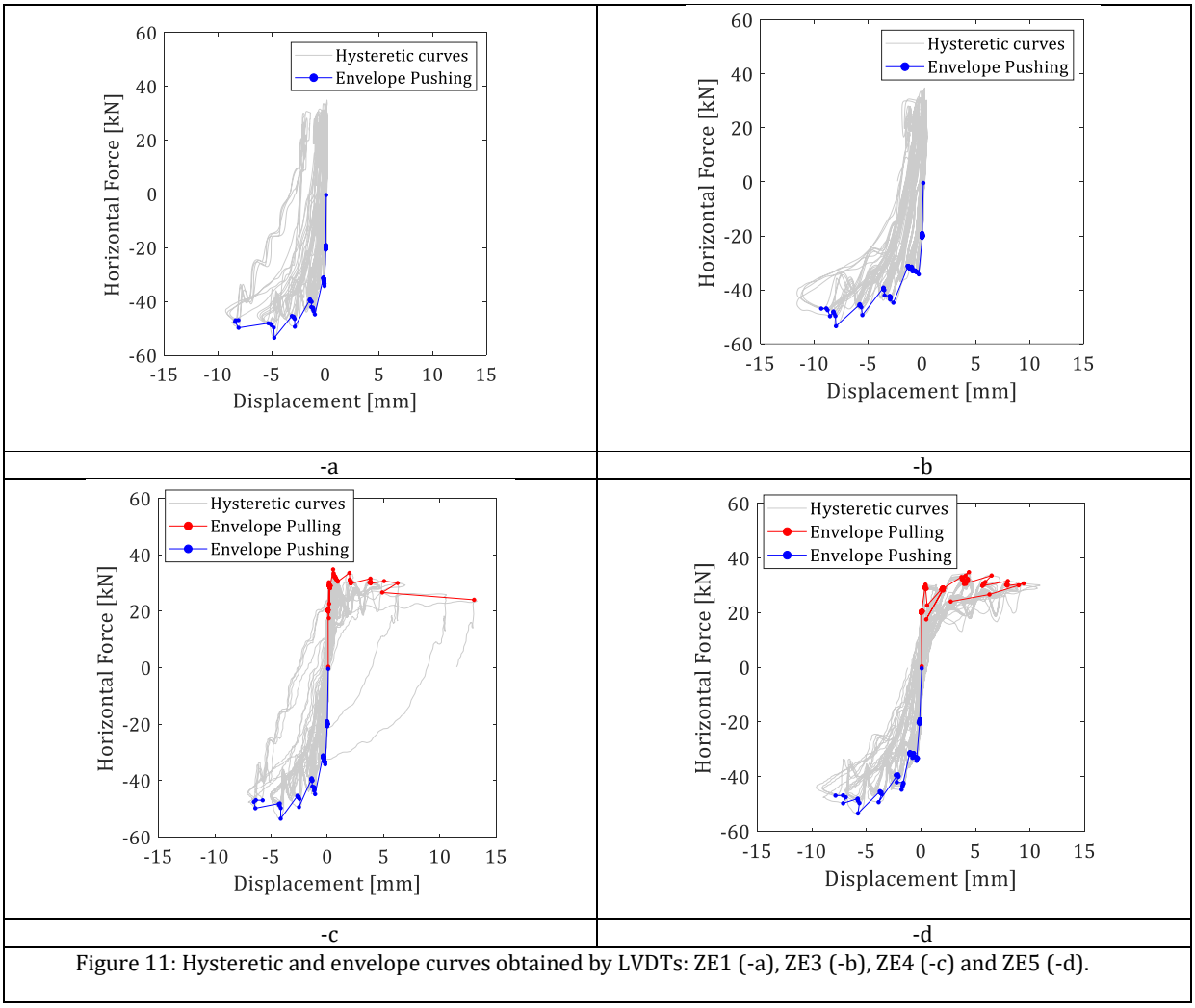

Figure 11: Hysteretic and envelope curves obtained by LVDTs: ZE1 (-a), ZE3 (-b), ZE4 (-c) and ZE5 (-d).

4.1.5 Cracking Mechanism

The displacement histories from all the LVDTs on Walls B and C are depicted in Figure 12 and Figure 13, respectively. Figure 12-a shows the relative displacement between Walls A and B. LVDTs 19 and 20 detected negligible displacements under both pulling and pushing loads, while 18 detected a maximum displacement under pulling loads of approximately 12 mm at the end of the test. A similar trend can also be seen in Figure 13-a, which gives the values of the LVDTs between Walls A and C. LVTD 9 shows a maximum displacement of 12 mm, unlike LVDT 18, 9 started to record non-negligible displacement values after the 200th cycle instead of the 125th (as in LVDT 18), which confirmed that damage first appeared in Wall B, which had a higher opening ratio. This crack pattern not only affected Wall B but also worsened the out-of-plane behaviour of A. Since LVDTs 18, 19, 20, 9, 10 and 11 were equally spaced along the panels, it can be concluded that only the upper third of a masonry building is highly vulnerable to horizontal loads when the roof is totally disconnected from the load-bearing walls.

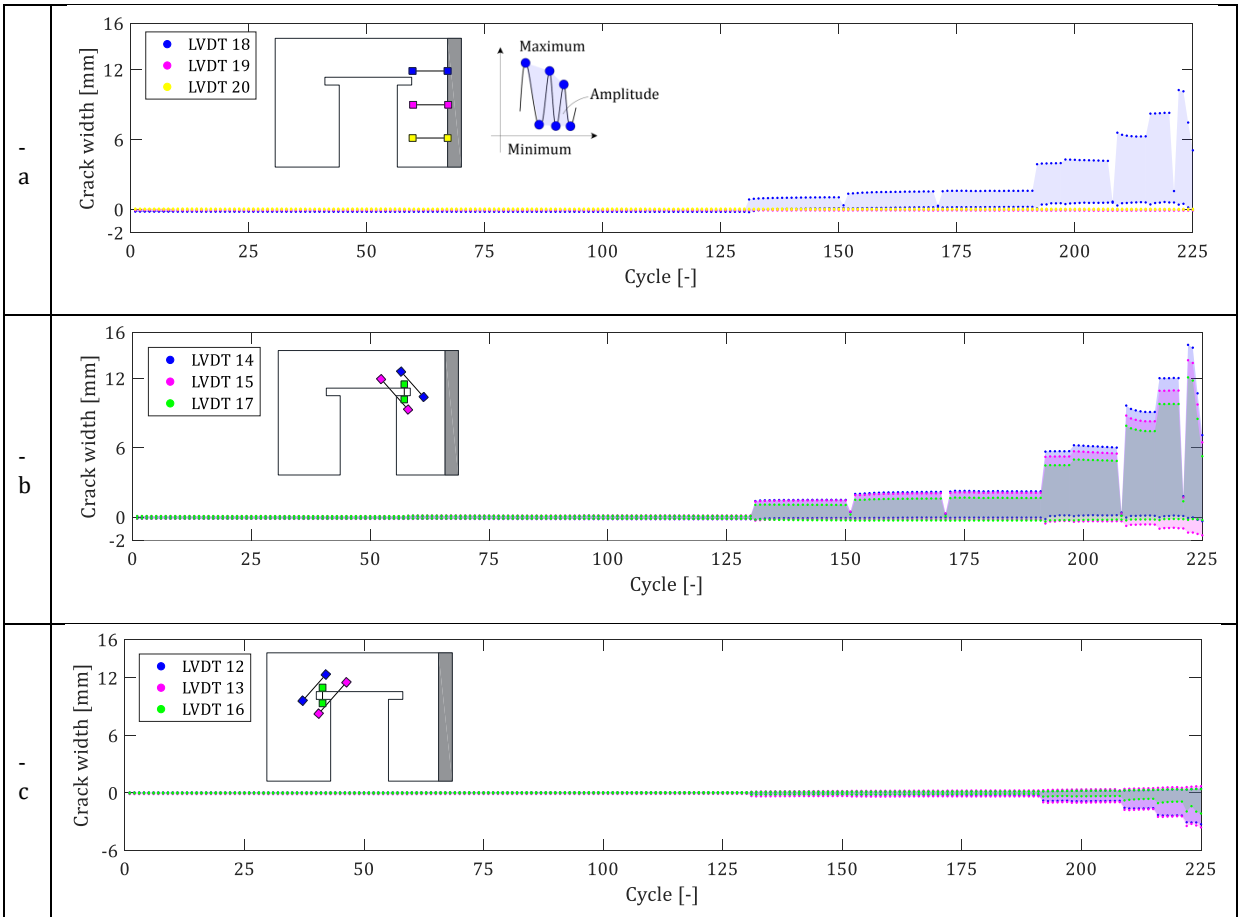

Figure 12: Cracks width in Wall B: Walls A and B (-a), door right upper corner (-b), door left upper corner (-c).

Figure 12-b and –c show the displacement histories monitored by the LVDTs in the door corners. The cracking mechanism, which formed around the 125th cycle, mostly affected the right side of Wall B. The cracks appeared in the right corner between the wooden lintel and the masonry and propagated in a zigzag until they affected the loading system. Similar behaviour was observed in Wall C. LVDTs 4, 8, 5 and 6 were placed on the right side of the window opening. As can be seen in Figure 13-b, the LVDTs in the upper right corner detected a maximum crack opening of almost 12 mm, whereas LVDT 6 detected 3 mm of maximum displacement, indicating that the crack pattern formed in the upper corner while the lower one escaped almost unaffected. Conversely, all the LVDTs in the left corner detected two cracking mechanisms: one in the lower corner (LVDT 3) and another in the upper corner (LVDTs 1 and 2), as can be seen in Figure 13-c.

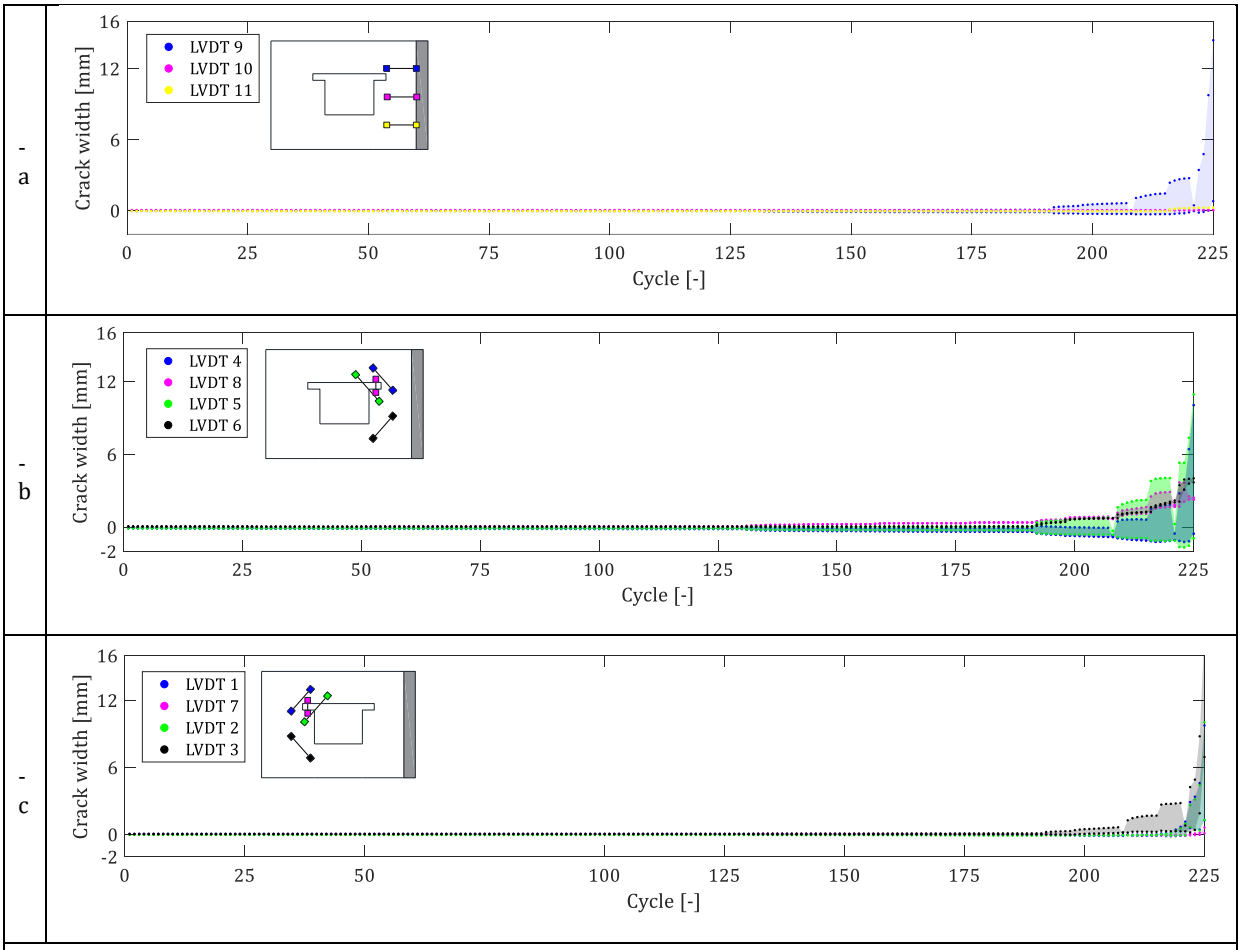

Figure 13: Crack width in Wall C: Walls A and C (-a), right corner (-b), left corner (-c).

The cracking mechanisms in Walls B and C at the end of the test are shown in Figure 14-a and –b, respectively. Figure 14 gives the cumulative residual crack openings detected by all the LVDTs on both side walls. As clearly visible, Wall C experienced serious damage, mostly in the lower left (20 mm) and upper corners (approximately 10 mm). The LVDTs on Wall B recorded a final maximum residual crack widening of 2.5 mm only in the right upper corner. In both these areas, stepped cracks formed in the corners of the openings and propagated along the mortar joints until they connected with the loading system (Figure 14).

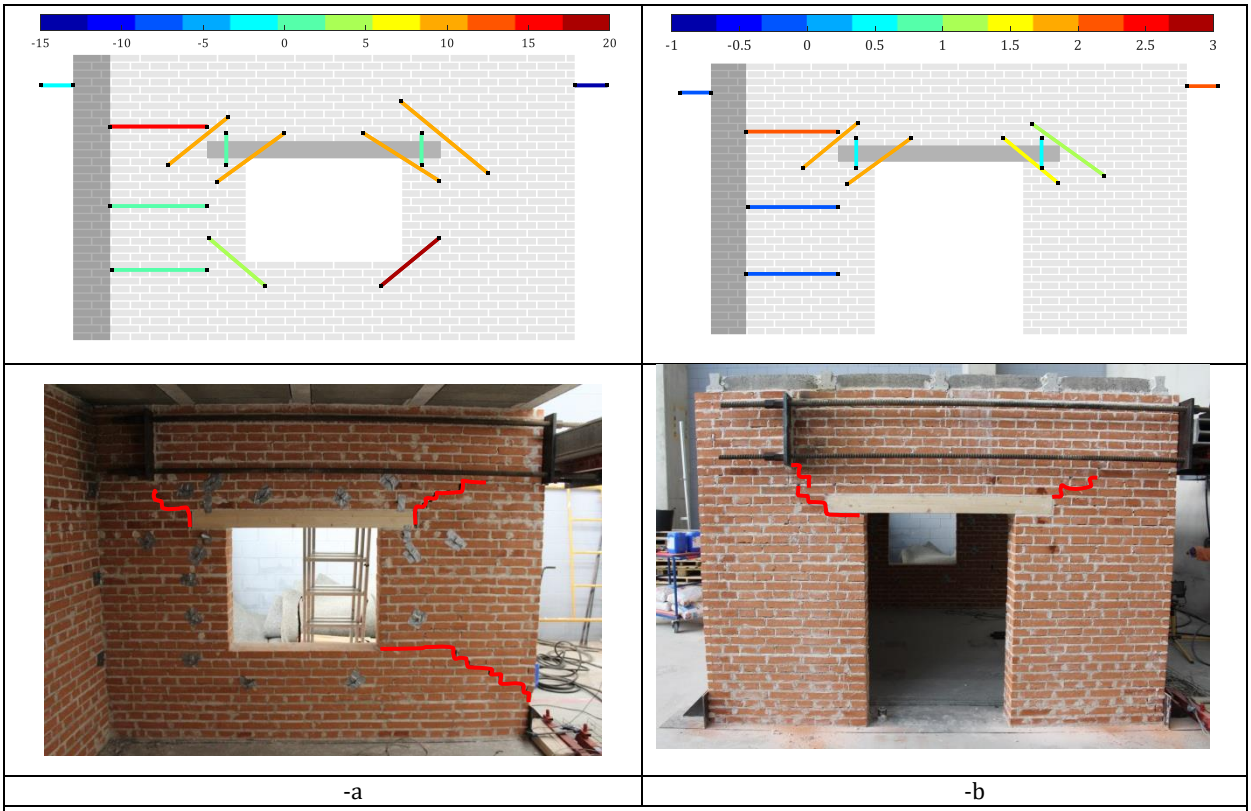

-a -b

Figure 14: Cumulative residual crack widening [mm] at the end of the test: Wall C (-a) and Wall B (-b) with their cracking patterns.

4.2 TRM Reinforced Prototype

4.2.1 Strength Degradation

The TRM (Textile Reinforced Mortar) reinforced structure was subjected to a total of 149 cycles subdivided into seven different sets of imposed displacement. The results of the strength degradation obtained for pulling and pushing loads are shown in Figure 15. Comparing Figure 7 and Figure 15, the TRM strengthening helped not only to completely restore the original load-bearing capacity of the building but also increased it by 25% more than the as-built case when ±1 mm was applied to the prototype. The same proportion was maintained with double the imposed displacement (± 2 mm), meaning that the TRM-reinforced structure behaved elastically under both pulling and pushing actions.

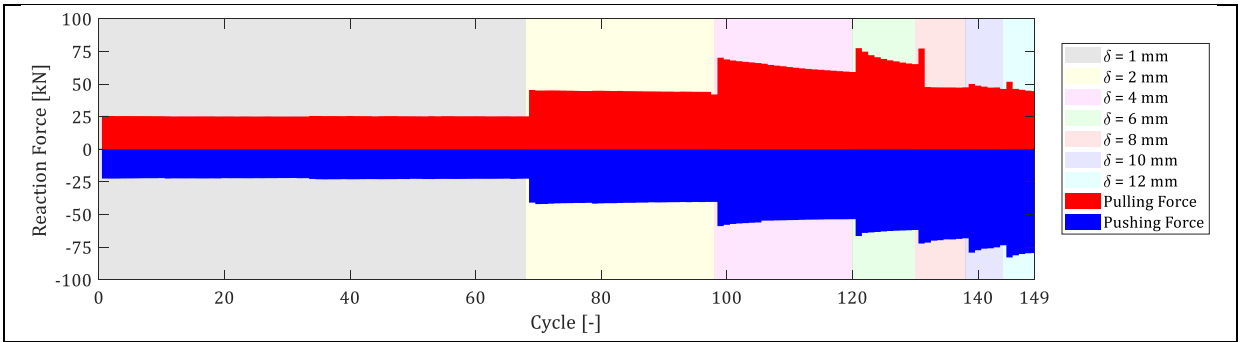

Figure 15: Strength degradation obtained testing the TRM reinforced building.

Different strength degradation trends appeared after ±4 mm, as in the as-built structure. The TRM-reinforced building had markedly different behaviour under pushing and pulling loads. Under pushing loads, the strength deterioration curves steepened with the number of cycles in each set of displacements, while under pulling loads, strength degradation appeared up to 6 mm. In the subsequent steps (after 8 mm), the damage close to the loading areas in Wall B threatened the transmission of the pulling loads and there was a negligible increase in the peak forces. Figure 7 and Figure 15 show the influence of TRM in improving the displacement capacity of the masonry structure under pulling loads. Indeed, the TRM-reinforced structure experienced a non-proportional increased peak force due to the greater applied displacement. This behaviour was not observed in the as-built prototype, in which the peak forces continued to degrade with approximately the same trend from 8 mm to the end of the test.

4.2.2 Pinching Effect

The pinched response of the TRM reinforced prototype in Figure 16 considers all the LVDTs placed parallel to the side walls. As expected, no pinching occurred at low imposed displacement values (i.e. till 4 mm), after which the prototype's structural response started to experience considerable inelastic displacements as shown by the force-displacement curves. This phenomenon is particularly visible in the pushing loads given in Figure 16. It is important to note that the prototype also experienced clear torsional effects with higher displacements in Wall B (Figure 16-b and -d) than C (Figure 16-a and –c). Unlike the as-built case, the TRM played an important role during pulling loads. There was quite a big difference between the displacements read by LVDTs ZE1, ZE3 and ZE4 and ZE5. This apparently different response was due to a deep crack in the upper right corner of Wall B, made the loading system rotate around the central hinge and concentrated the imposed displacements on that side (Figure 16-d). However, higher overall displacements occurred in the TRM-reinforced prototype under pushing loads than in the control building, indicating that TRM can extend the displacement capacity of brittle masonries subjected to seismic movements.

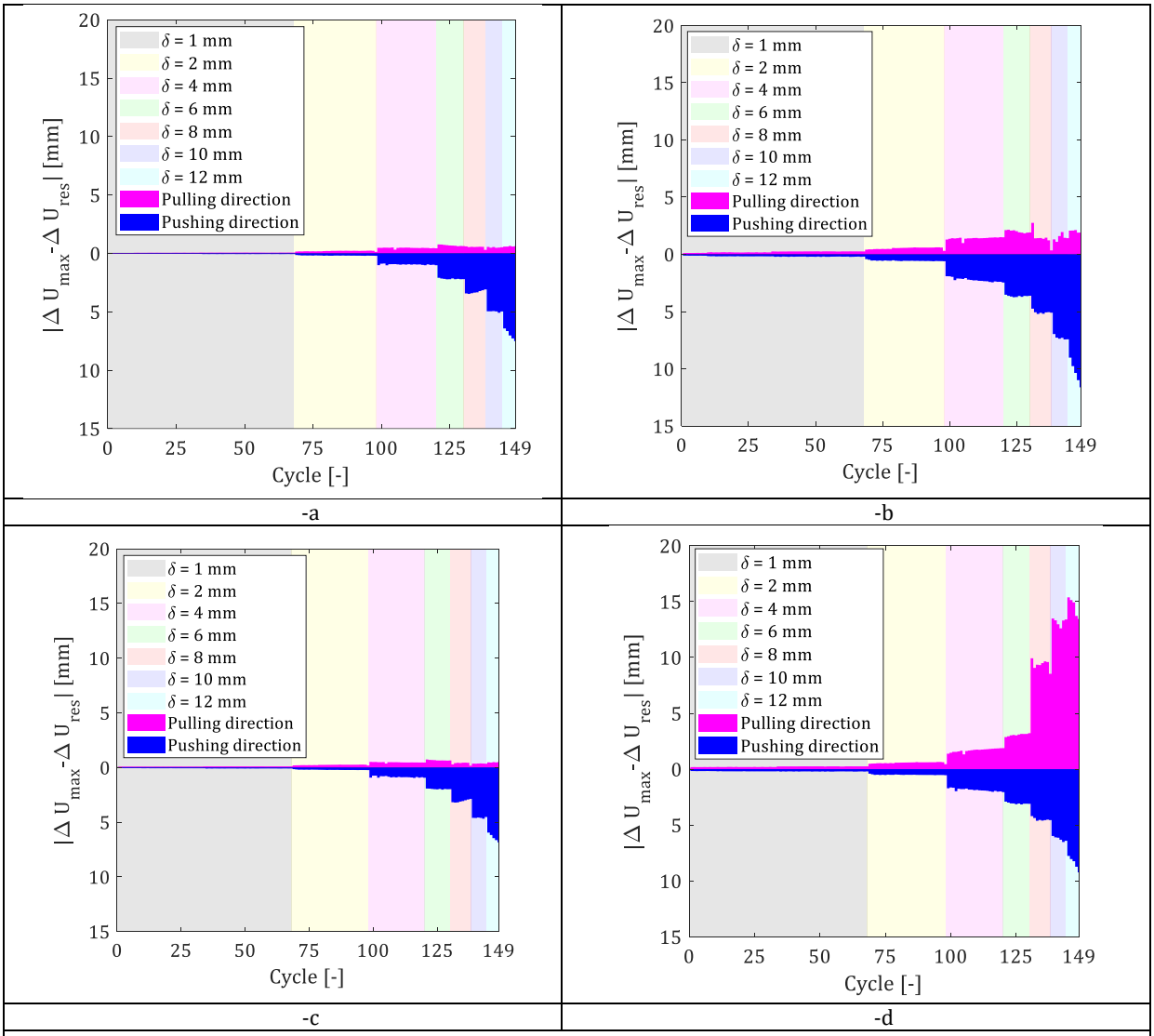

Figure 16: Pinching effect computed from LVDTs: ZE1 (-a), ZE3 (-b), ZE4 (-c) and ZE5 (-d).

Similar outcomes can be seen in the force-displacement curves obtained by the LVDTs at the end of each set of imposed displacements (Figure 17). Pinched curves started to appear during the third set (4 mm) until the end of the test under pushing loads. The building's response was greatly affected by the induced rotation of the loading system, as shown by the low horizontal displacement values.

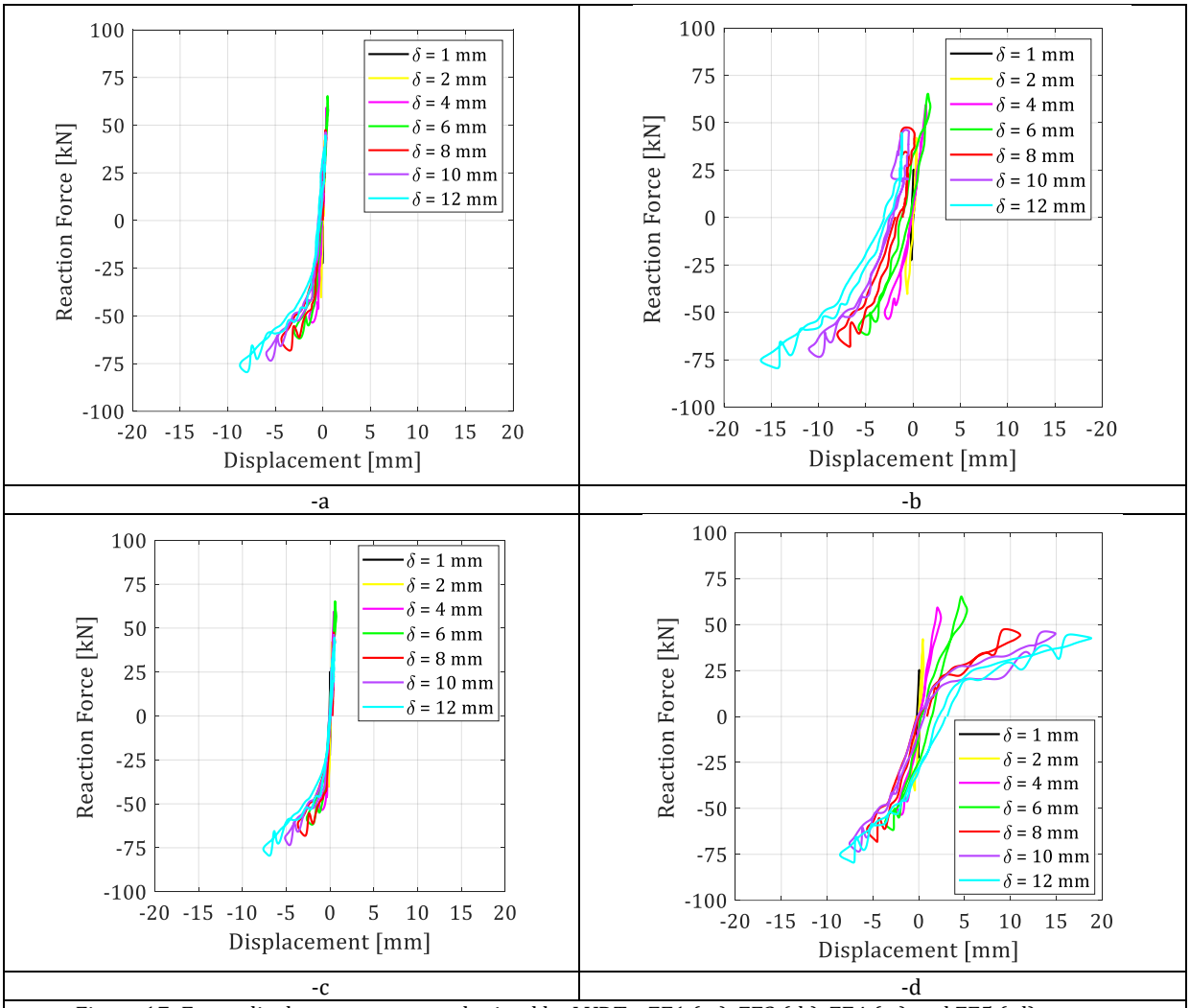

Figure 17: Force-displacement curves obtained by LVDTs: ZE1 (-a), ZE3 (-b), ZE4 (-c) and ZE5 (-d).

4.2.3 Cumulative Energy Dissipation

The Cumulative Energy Dissipations (CED) obtained in the reinforced structure are given in Figure 18. Comparing Figure 10 with Figure 18, similar CED values were obtained at the end of both tests, which, together with the few cracks on the applied TRM composite shows that the TRM was able to maintain the building's dissipation capacity and helped to delay the formation of severe cracking patterns. Unlike the as-built prototype, the reinforced structure showed a more regular energy dissipation rate, passing from one set of imposed displacements to another, and induced monolithic behaviour in which the side walls collaborated in sustaining the external action.

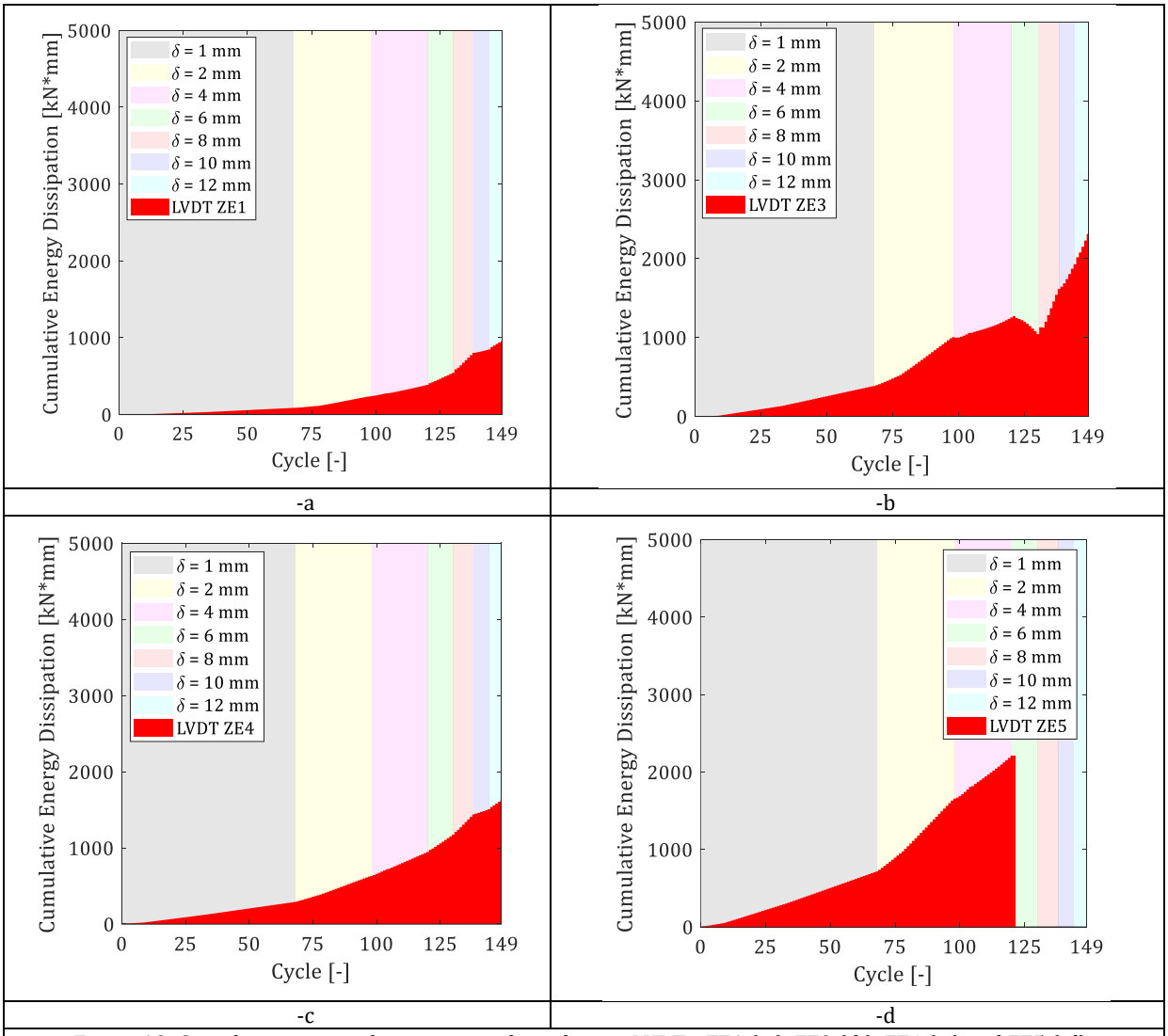

Figure 18: Cumulative energy dissipation evaluated using LVDTs: ZE1 (-a), ZE3 (-b), ZE4 (-c) and ZE5 (-d).

4.2.4 Envelopes

The envelope curves deduced from the hysteretic loops obtained by ZE1, ZE3, ZE4 and ZE5 in the reinforced structure are given in Figure 19. As in the as-built case, Figure 19-a and –b gives the skeleton curves only under the pushing loads superimposed on the hysteretic loops obtained experimentally, while Figure 19-c and –d shows the complete envelope curves for both pushing and pulling actions obtained from the two LVDTs on the loading-system side of the masonry prototype.

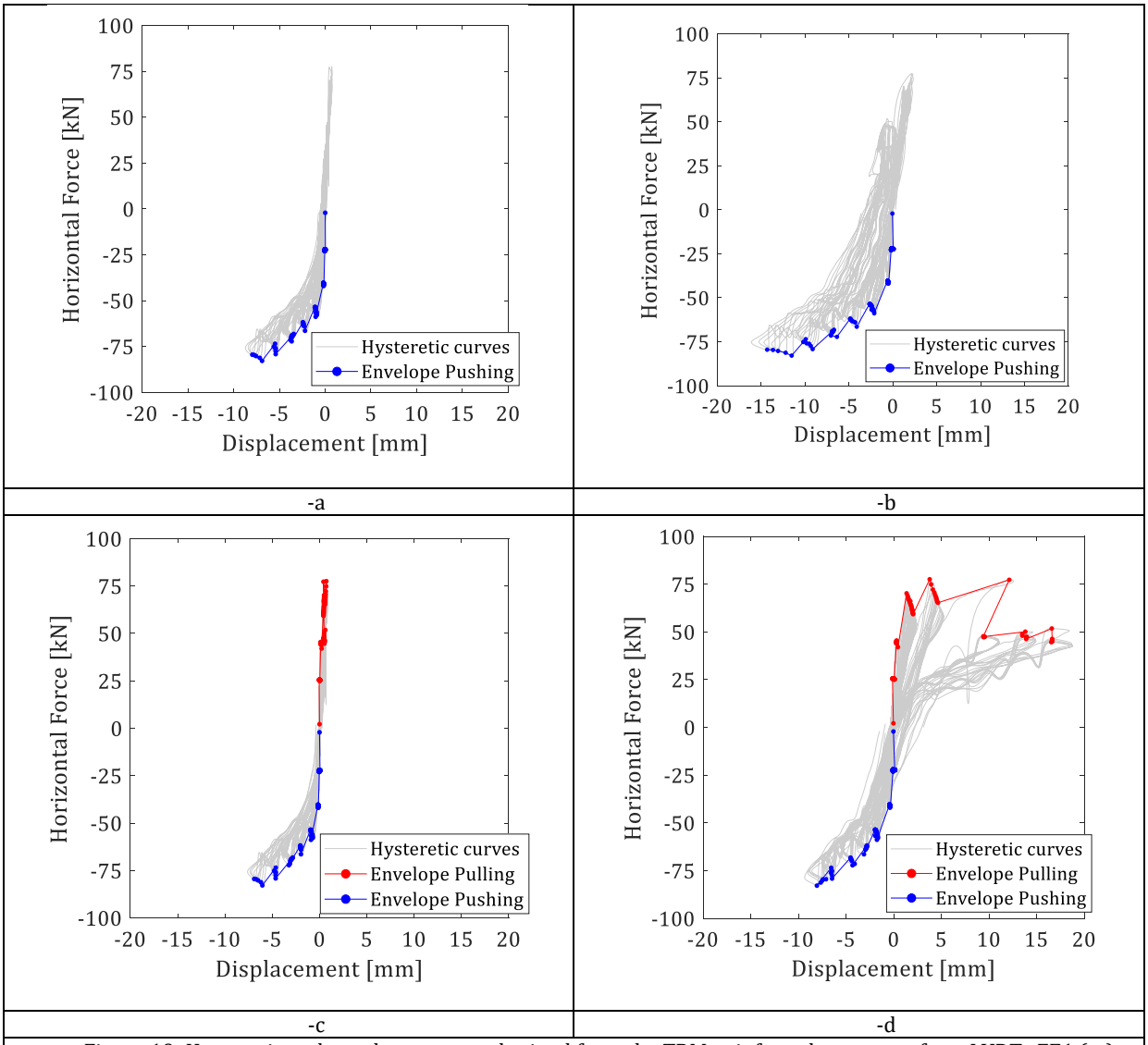

Figure 19: Hysteretic and envelope curves obtained from the TRM-reinforced prototype from LVDTs ZE1 (-a), ZE3 (-b), ZE4 (-c) and ZE5 (-d).

The behaviour of the reinforced building under pushing loads showed quite a large increase of the reaction forces, which passed from approximately 60 kN in the as-built to almost 85 kN in the reinforced structure. Non-negligible differences were found when pulling loads were applied to the masonry prototype, as can be seen in Figure 11-c and –d with Figure 19-c and –d. The opening of a deep crack in Wall B of the reinforced structure, close to the gripping area induced the rotation of the loading system around the central hinge and thus helped to concentrate the imposed displacements on that side (Figure 19-d). The apparently low displacement values shown in Figure 19-c can be explained by the adverse effects of damage to the stiff beam connected to the loading system. The skeleton curves obtained under pushing loads were not affected by this problem.

4.2.5 Cracking Mechanism

The crack opening histories detected by all the LVDTs on Walls B and C of the reinforced structure are given in Figure 20 and Figure 21, respectively. In Figure 20-a and -b LVDT 18 detected the formation of a crack approximately around the 100th cycle, which started close to the right upper corner of the door opening and propagated as far as the gripping plate. The crack formation was tracked by LVDTs 14 and 15 and had a maximum opening of approximately 28 mm and also influenced the out-of-plane behaviour of the solid wall, on which LVDT 18 registered a maximum relative displacement of 18 mm.

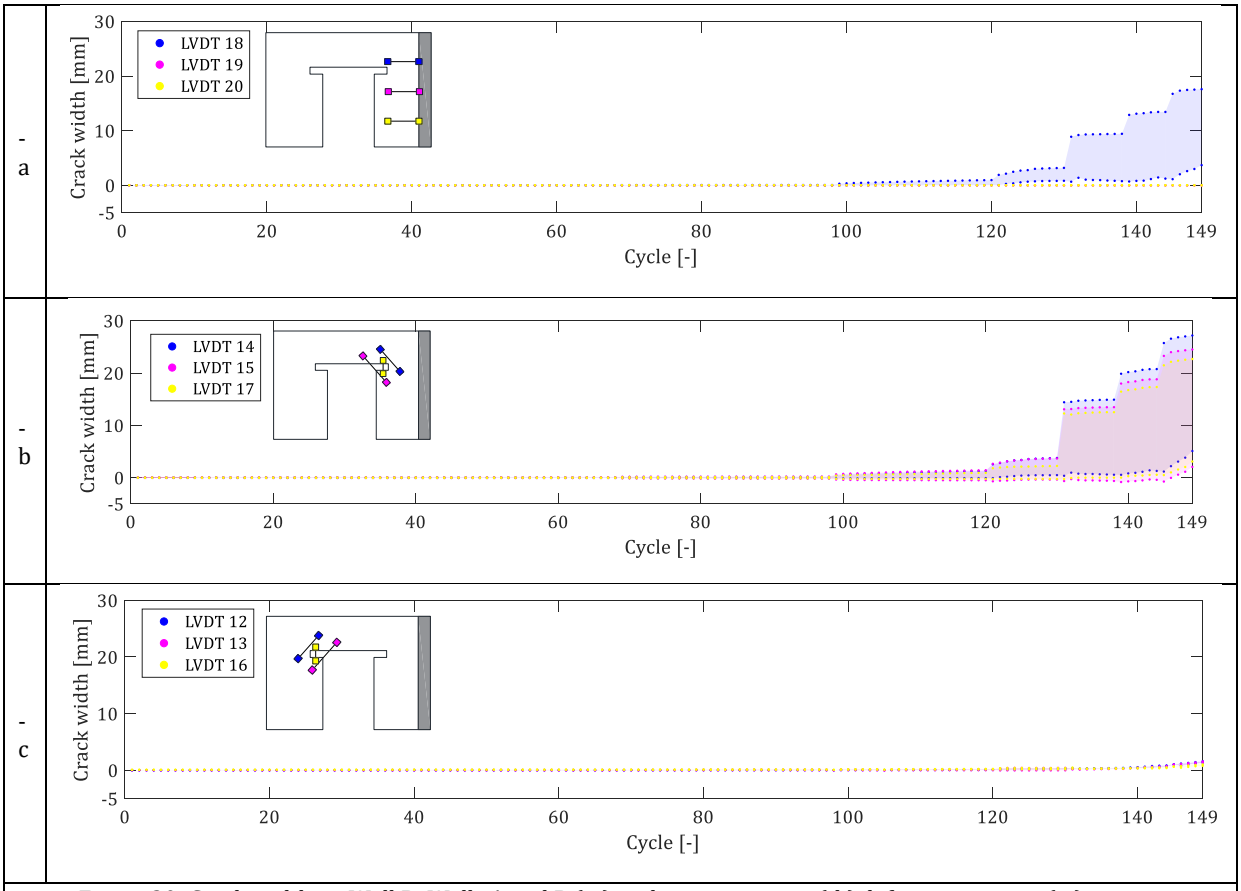

Figure 20: Crack width on Wall B: Walls A and B (-a), right upper corner (-b), left upper corner (-c).

LVDTs 12, 13 and 16 detected negligible displacements, meaning that no cracks formed on that side, nor was Wall C affected by damage mechanisms, as confirmed by the displacements monitored by all the LVDTs between Walls A and C (Figure 21-a) as well as around the corners of the opening (Figure 21-b and -c). These findings were further confirmed by the residual crack openings depicted in Figure 22. Wall C experienced no cracking mechanism, while major damage was found on Wall B. No debonding failures were found at the end of the test. Matrix cracking and tensile failure of the glass grid were detected in the repaired zone on the upper-right of Wall B (Figure 22-b). The effect of the TRM strengthening can be evaluated from the following aspects: (i) it changed the building behaviour to monolithic in which all the walls

collaborated in sustaining the external actions, (ii) the as-built structure experienced the formation of various narrow cracks in both side walls (maximum 16mm), (iii) the TRM-reinforced structure experienced more local damage (Wall B only) with wider crack openings (almost 28 mm), (iv) comparing the cycle at which cracks formed, it can be concluded that the as-built structure experienced damage around the 125th cycle (2 mm imposed displacement) while the opening of cracks was delayed by the TRM composite until the 100th cycle (4 mm imposed displacement), and (v) the TRM helped to completely restore the original continuity of the severely damaged masonry building.

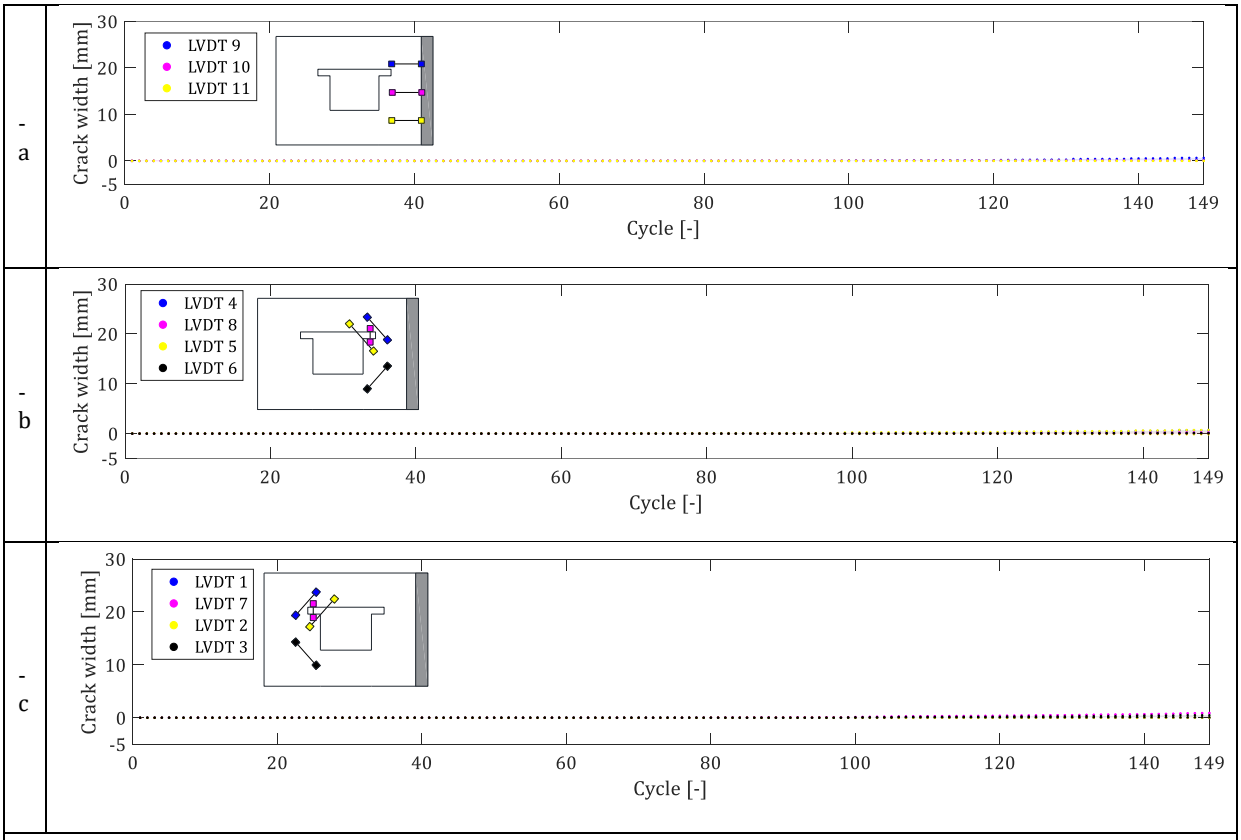

Figure 21: Crack width Wall B: Walls A and B (-a), right corner (-b), left corner (-c).

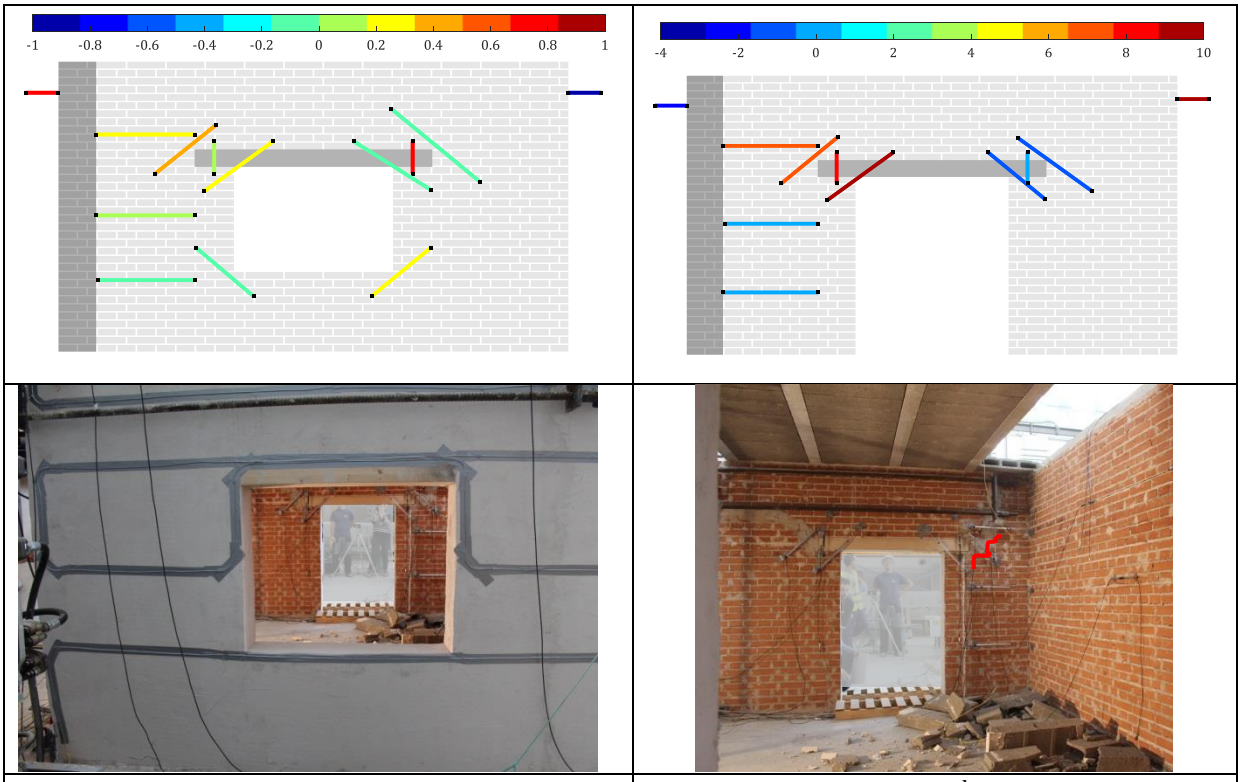

-a -b

Figure 22: Cumulative residual crack widening [mm] at the end of the test in the TRM-reinforced structure: Wall C (-a) and Wall B panel (-b) with cracking patterns.

5. Conclusions

The paper describes the experimental testing of a 2/3-scale U-shaped masonry building subjected to pseudo-dynamic horizontal loads to analyse the seismic response of weak low-rise masonries with flexible diaphragms, no box behaviour and moderate torsional effects, and the effectiveness of Textile Reinforced Matrix composites as a strengthening alternative for the repair of severely damaged structures. From the results obtained the following conclusions can be drawn:

- A total of 6 (225 cycles) and 7 (149 cycles) series of pseudo-dynamic excitations each lasting 10 seconds were applied to the unreinforced (URM) and TRM-strengthened structures.
- The structural response of the as-built and TRM-reinforced structures were quite symmetric in terms of peak forces at low values of imposed displacement (up to 2 mm);
- TRM strengthening helped to completely restore the original load-bearing capacity of the building and increased it by 25% more than the as-built case when ±1 mm was applied to the prototype.

- Two mechanisms were observed in both the as-built and repaired structures from 4 mm until the end of the test: (i) the reaction forces increased with the imposed displacement, but not in proportion, and (ii) different strength degradation trends were found at each level of imposed displacement.
- TRM helped to restore the original continuity of the severely damaged masonry building.
- TRM strengthening changed the behaviour of the building to monolithic, in which all the walls collaborated in sustaining the external actions.
- The as-built structure experienced the formation of various narrow cracks in both side walls (maximum 16mm), while the TRM-reinforced structure experienced more local damage (Wall B only) with wider crack openings (almost 28 mm).
- The as-built structure sustained damage around the 125th cycle (2 mm imposed displacement). In the second test the cracks were delayed by the TRM composite until the 100th cycle (4 mm imposed displacement);
- TRM composites influenced the energy dissipation capacity of the masonry structure, delayed the plastic dissipation stage, and had a negligible effect on Cumulative Energy Dissipation.
- Future research will be devoted to the evaluation and comparison of the experimental results by means of numerical modelling.

6. References

[1] S. Kallioras, G.Guerrini, U. Tomassetti, B.Marchesi, A. Penna, F. Graziotti, G. Magenes, Experimental seismic performance of a full-scale unreinforced clay-masonry building with flexible timber diaphragms, Engineering Structures 161 (2018) 231-249.

[2] F. Graziotti, U. Tomassetti, A. Penna, G. Magenes, Out-of-plane shaking table test on URM single leaf and cavity walls, Engineering Structures 125 (2016) 455-470.

[3] P.X. Candeias, A. Campos Costa, N. Mendes, A.A. Costa, P.B. Lourenço, Experimental Assessment of the Out-of-Plane Performance of Masonry Buildings Through Shaking Table Tests, Int. J. Archit. Herit. 11 (2017) 31–58.

[4] Y.H. MugahedAmran, R. Alyousef, R.S.M. Rashid, H. Alabduljabbar, C.-C. Hung, Properties and applications of FRP in strengthening RC structures: A review, Structures. 16 (2018) 208–238.

[5] L.A.S. Kouris, T.C. Triantafillou, State-of-the-art on strengthening of masonry structures with textile reinforced mortar (TRM), Constr. Build. Mater. 188 (2018) 1221–1233.

[6] N. Spinella, Modeling of shear behavior of reinforced concrete beams strengthened with FRP, Compos. Struct. 215 (2019) 351–364. doi:10.1016/j.compstruct.2019.02.073.

[7] A. Siddika, M.A. Al Mamun, R. Alyousef, Y.H.M. Amran, Strengthening of reinforced concrete beams by using fiber-reinforced polymer composites: A review, J. Build. Eng. 25 (2019) 100798. doi:10.1016/j.jobe.2019.100798.

[8] F.M. Mukhtar, R.M. Faysal, A review of test methods for studying the FRP-concrete interfacial bond behavior, Constr. Build. Mater. 169 (2018) 877–887. doi:10.1016/j.conbuildmat.2018.02.163.

[9] E. Bernat-Masó, L. Gil, Assessing the performance of CFRP strengthening on masonry walls using experimental modal analysis, Eng. Struct. 193 (2019) 184–193. doi:10.1016/j.engstruct.2019.05.036.

[10] S.A. Babatunde, Review of strengthening techniques for masonry using fiber reinforced polymers, Compos. Struct. 161 (2017) 246–255. doi:10.1016/j.compstruct.2016.10.132.

[11] F. Freddi, E. Sacco, Debonding Process of Masonry Element Strengthened with FRP, Procedia Eng. 109 (2015) 27–34. doi:10.1016/j.proeng.2015.06.206.

[12] F. Ceroni, M. Leone, V. Rizzo, A. Bellini, C. Mazzotti, Influence of mortar joints on the behaviour of FRP materials bonded to different masonry substrates, Eng. Struct. 153 (2017) 550–568. doi:10.1016/j.engstruct.2017.10.030.

[13] P. Carrara, D. Ferretti, F. Freddi, Debonding behavior of ancient masonry elements strengthened with CFRP sheets, Compos. Part B Eng. 45 (2013) 800–810. doi:10.1016/j.compositesb.2012.04.029.

[14] DPCM 09/02/11. Evaluation and reduction of seismic risk of cultural heritage with reference to the Technical Standards for Constructions promulgated by the Ministry of Infrastructure and Transport on 2008 January 14th; 2011.

[15] C.G. Papanicolaou, T.C. Triantafillou, K. Karlos, M. Papathanasiou, Textile-reinforced mortar (TRM) versus FRP as strengthening material of URM walls: in-plane cyclic loading, Mater. Struct. 40 (2007) 1081–1097. doi:10.1617/s11527-006-9207-8.

[16] C.G. Papanicolaou, T.C. Triantafillou, M. Papathanasiou, K. Karlos, Textile reinforced mortar (TRM) versus FRP as strengthening material of URM walls: Out-

of-plane cyclic loading, Mater. Struct. Constr. 41 (2008) 143–157. doi:10.1617/s11527-007-9226-0.

[17] M. Harajli, H. ElKhatib, J.T. San-Jose, Static and Cyclic Out-of-Plane Response of Masonry Walls Strengthened Using Textile-Mortar System, J. Mater. Civ. Eng. 22 (2010) 1171–1180. doi:10.1061/(asce)mt.1943-5533.0000128.

[18] S. De Santis, P. Casadei, G. De Canio, G. de Felice, M. Malena, M. Mongelli, I. Roselli, Seismic performance of masonry walls retrofitted with steel reinforced grout, Earthq. Eng. Struct. Dyn. 45 (2016) 229–251. doi:10.1002/eqe.2625.

[19] M. Shabdin, M. Zargaran, N.K.A. Attari, Experimental diagonal tension (shear) test of Un-Reinforced Masonry (URM) walls strengthened with textile reinforced mortar (TRM), Constr. Build. Mater. 164 (2018) 704–715.

[20] Z. Al-Jaberi, J.J. Myers, M.A. ElGawady, Pseudo-static cyclic loading comparison of reinforced masonry walls strengthened with FRCM or NSM FRP, Construction and Building Materials 167 (2018) 482-495.

[21] M. Deng, S. Yang, Cyclic testing of unreinforced masonry walls retrofitted with engineered cementitious composites, Construction and Building Materials 177 (2018) 395-408.

[22] M. Deng,Z. Dong,X. Wang,Y. Zhang,T. Zhou, Shaking table tests of a half-scale 2-storey URM building retrofitted with a high ductility fibre reinforced concrete overlay system, Engineering Structures 197 (2019) 109424.

[23] R. Bairrao, M.J.F. Silva, Shaking table tests of two different reinforcement techniques using polymeric grids on an asymmetric limestone full-scaled structure, Engineering Structures 31 (2009) 1321-1330.

[24] MAPEI, (2018) http://www.mapei.com/.

[25] EN 14580. Natural stone test methods. Determination of the static elastic moduls, (2005).

[26] EN 13412. Products and systems for the protection and repair of concrete structures - Test methods - Determination of modulus of elasticity in compression, (2008).

[27] EN 1015-11. Methods of test for mortar for masonry Determination of flexural and compressive strength of hardened mortar, (1999).